Atomic processes of shear-coupled migration in {112} twins and vicinal grain boundaries in bcc-Fe

N. Kvashin,[1] P. L. García-Müller,[2] N. Anento,[1] and A. Serra[1]
[1]*Department of Civil and Environmental Engineering, Universitat Politècnica de Catalunya, 08034 Barcelona, Spain*
[2]*CIEMAT, Avda. Complutense 40, Madrid 28040 Spain*

(Received 21 January 2020; revised 11 June 2020; accepted 19 June 2020; published 15 July 2020)

Tilt {112} grain boundaries (GBs) in bcc metals perform shear-coupled grain-boundary migration by the creation and glide of disconnections. Disconnection dipoles may be created at the pristine GB at high stresses or may be generated at the core of a GB dislocation that acts as a source of disconnections. We characterize this source in terms of its Burgers vector, denoted $\vec{b}_{1/-1}$, and describe the mechanism that allows the source to move conservatively with the GB. The $\vec{b}_{1/-1}$ grain-boundary dislocation is created, for instance, during the absorption of a crystal dislocation by the {112} grain boundary. In addition, $\vec{b}_{1/-1}$ accommodates {112} vicinal grain boundaries that are formed by segments of {112} planes separated by $\vec{b}_{1/-1}$ grain-boundary dislocations. The presence of these $\vec{b}_{1/-1}$ dislocations facilitates the conservative displacement of both the pristine and the vicinal GBs. We show that the creation of disconnections is the key for the absorption of edge and screw dislocations by the GB and the drag of mixed dislocations by the GB during its migration. These conservative processes are efficient ways to accommodate plastic deformation by the growth and shrink of {112} twins, and shear-coupled motion of the {112} GB and its vicinal GBs.

DOI: 10.1103/PhysRevMaterials.4.073604

I. INTRODUCTION

Grain-boundary (GB) migration under stress is an important plastic deformation mechanism that has been studied both experimentally and by computer simulation [1–15]. The migration occurs by the glide of disconnections (GB line defects with both dislocation and step character) along the GB [7–15]. Thus, the effectiveness of the accommodation of plastic deformation depends on the creation of disconnections, its glissile character, and the interaction of these disconnections with other defects lying on the GB. Disconnections can be created, either directly as dipoles at the GB or by defects at the GB acting as sources of disconnections. For these sources to be efficient, they must move together with the GB. Whether the process is conservative or not depends on the crystallography of both the GB and the source of disconnections. The most efficient process that leads to a shear-coupled GB migration is conservative, i.e., no atomic diffusion is needed; moreover, the process must be sustained by the continuous creation of disconnections. A well-known example is the shear-coupled migration of the (10–12) twin boundary that occurs in all hexagonal-closed-packed (hcp) metals [12,13]. In the face-centered-cubic (fcc) metals, Combe *et al.* [14] studied a new GB migration mechanism through the nucleation of a mobile disconnection from the sessile one in the (410) tilt GB. Bristowe and Crocker [15] suggested the heterogeneous creation of disconnections in a pioneering study of twin boundary dislocations (referred as twinning dislocations) in the {211} twin boundary in body-centered-cubic (bcc) metals. More recently, Gumbsch and collaborators [16,17] studied the interaction of 1/2(111) dislocations with the {112} tilt GBs in bcc tungsten. They reported transmission or absorption, depending on the character of the dislocation, but it was not found a source of disconnections that would facilitate the continuous GB migration. Finally, Jiang *et al.* [18] have presented an experimental evidence using *in situ* high-resolution transmission electron microscopy (HRTEM), of the growth of deformation twins in bcc tantalum and niobium. To analyze the growth mechanism they performed molecular dynamics (MD) simulations but only a particular case was presented where a dislocation with Burgers vector (Bv) parallel to the interface has to interact with a disconnection of screw orientation for the growth to occur.

In this paper we describe, in terms of dislocation reactions, based on the theory of interfacial defects [19–21], a GB dislocation (GBD) acting as a source of disconnections that operates in the (112) tilt GB and in the GBs vicinal to the (112) GB, i.e., GBs obtained by increasing slightly its misorientation.

We also describe the role of this GBD on the interaction of a crystal dislocation with the {112} GB. Grain boundaries and extended intragranular defects, such as deformation twins, limit the mobility of crystal dislocations. The first stage of plastic deformation is initiated by the motion of dislocations but the sustainability and capacity of controlled deformation depends on the propagation of slip through grains and, where appropriate, through extended twins [22,23].

The interactions of the family of 1/2(111) crystal dislocations with the (112) tilt GB in Fe are described in detail showing that they are related to the source of disconnections. In this paper we prove that the mechanism previously described for hcp and fcc metals occurs in bcc metals indicating that it is essentially controlled by the existence of the appropriate dislocation reactions at the GB expressed in terms of their Burgers vectors.

The {112} tilt GB has the lowest energy among the symmetric GBs with ⟨110⟩ tilt axis in bcc metals (the atoms at the GB have the perfect coordination number) [24,25]. Among

the symmetric tilt GBs, the $\Sigma 3\{112\}\langle 110\rangle$ GB has a special relevance because it is the coherent boundary of the {112} twin, which is the twin mode in bcc metals. The ease of twinning at high strain rate deformation or low temperature [26] is facilitated by the conservative shear-coupled twin boundary migration, as described below.

GBs vicinal to the low-index {112} GB are formed by a {112} GB with a misorientation angle modified by a small increment. These GBs are high-index boundaries and have higher energy formation. Under equilibrium conditions, they relax into segments of {112} GBs separated by GB dislocations accommodating the increase of misorientation. They may be understood as the superposition of {112} GB, with misorientation angle $\theta = 70.53°$ [24,25], and a low-angle GB formed by arrays of aligned crystal dislocations that have relaxed into GB dislocations [10].

II. GRAIN-BOUNDARY DISLOCATIONS AT THE {112} GB

According to the theory of interfacial defects [19–21,27], GBD are related to the difference of broken symmetries when the GB is created by joining two crystals (λ and μ). If $\vec{t}_\lambda$ and $\vec{t}_\mu$ are broken translation symmetries, then $\vec{b} = \vec{t}_\lambda - \vec{t}_\mu$ represents the Burgers vector of a possible GBD. As mentioned above, if the GBD steps the GB it is named disconnection. In some papers, disconnections are called "partial dislocations," but this notation is not appropriate. Disconnections are "perfect" in the sense that the interfacial structure is identical on either side of the discontinuity.

The admissible GBD for the {112} tilt GB can be identified easily using the dichromatic pattern associated to the interface, as shown in Fig. 1. This is the superposition of lattice sites of the two crystals [drawn as yellow (λ) and black (μ)] in their tilt related orientations, with the sites of the (112) plane of the two crystals in coincidence. Thus, any lattice site of the coincident plane may be taken as the origin of both $\vec{t}_\lambda$ and $\vec{t}_\mu$, therefore, the Bvs are represented by arrows that go from black to yellow sites. The height of the step associated to the disconnection is $h = \vec{n} \cdot (\vec{t}_\lambda + \vec{t}_\mu)/2$ where $\vec{n}$ is the normal to the GB plane. We adopt the notation $\vec{b}_{n/m}$ to refer to all dislocations, being n and m the number of planes of λ and μ along $\vec{t}_\lambda$ and $\vec{t}_\mu$, respectively. The crystal dislocations residing solely in one of the crystals, for instance the λ crystal, are denoted by $\vec{b}_{n/0}$ ($\vec{b}_{2/0}$ and $\vec{b}_{1/0}$ in this work). In the reactions involving dislocations, n and m are conserved separately. The unit cells of each crystal are superimposed in red (λ) and blue (μ), respectively. The unit cell of the λ crystal contains the two Bv of bulk dislocations ($\vec{b}_{2/0} = \frac{1}{2}[111]_\lambda$ and $\vec{b}_{1/0} = \frac{1}{2}[1\bar{1}1]_\lambda$), with edge and mixed orientations, respectively, that interact with the GB. Figure 1 shows five examples of possible Bv of disconnections (black arrows). In our simulations, only disconnections denoted $\vec{b}_{1/1}$ and $\vec{b}_{-1/-1}$ have been observed: $|\vec{b}_{1/1}| = \frac{\sqrt{3}}{6}a_0 = 0.827$ Å. In terms of the topological theory of interfaces, they are related to the translation vectors of the λ and μ crystals as $\vec{b}_{1/1} = \frac{1}{2}[1\bar{1}1]_\lambda - [010]_\mu$ and $\vec{b}_{-1/-1} = [010]_\lambda - \frac{1}{2}[1\bar{1}1]_\mu$. The disconnection denoted as $\vec{b}^{\alpha}_{2/2}$ is unstable and decomposes into two $\vec{b}_{1/1}$ that move apart. The disconnection denoted $\vec{b}^{\beta}_{2/2}$

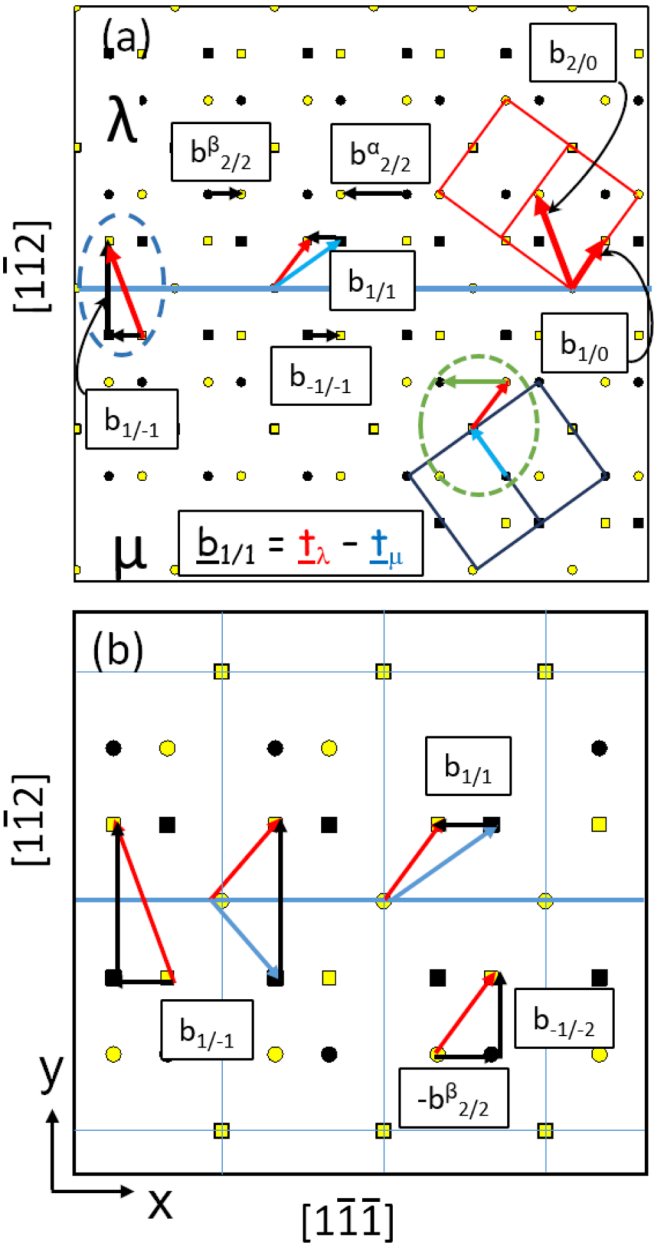

FIG. 1. (a) [1-10] projection of the dichromatic pattern associated with the (112) GB in Fe showing the Burgers vectors of the GB dislocations (black) and crystal dislocations (red and blue). (b) From left to right: decomposition of the edge dislocation ($b_{2/0}$) into GBD and disconnection; GBD and disconnection expressed as difference of translation vectors of λ and μ crystals. Possible decomposition of the mixed dislocation ($b_{1/0}$) into two GBDs.

is sessile. Thus, $\vec{b}_{1/1}$ disconnections are glissile, they have small Bv ($\frac{1}{3}$ of the Bv of the $\frac{1}{2}\langle 111\rangle$ bulk dislocation) and a step high of one (112) interplanar distance, which means that no shuffles are required during glide [28]. The resolved shear stress is around 20 MPa [29]. The GBD denoted as $\vec{b}_{1/-1}$ (encircled by blue dashed line in Fig. 1) has its Bv perpendicular to the GB and does not step the GB ($h = 0$). Since we describe essentially two GBD, hereafter the one that does not step the GB is denoted as "GBD" ($\vec{b}_{1/-1}$) and the

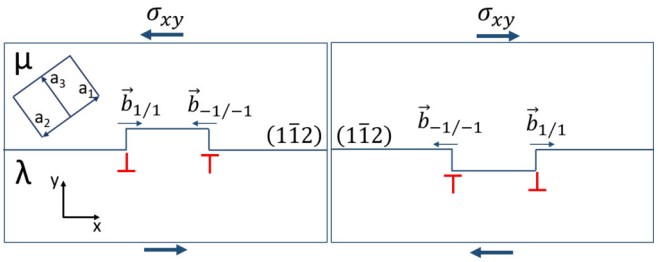

FIG. 2. Schematic of the bicrystal showing the unit cell of the upper crystal (μ) and the disconnection dipoles created under applied shear stress.

one that steps the GB is denoted as "disconnection" ($\vec{b}_{1/1}$ and $\vec{b}_{-1/-1}$).

III. SIMULATION METHOD

Molecular dynamics simulator LAMMPS [30] has been applied to study the atomic scale processes at the (1-12) GB and vicinal GBs. The simulations are performed at $T = 0$ K. The open visualization tool OVITO is used for visualization and analysis of atomistic simulation data [31]. The simulation box is oriented along $X =$ [1-1-1]; $Y =$ [1-12], and $Z =$ [110] directions with respective lengths 792.3, 283.5, and 16.13 Å and 300 668 atoms. To study the vicinal GBs the dimensions are slightly smaller: 778.3, 285.2, and 16.13 Å and 298 472 atoms. The boundary conditions were fixed in Y direction and periodic in the other directions. Two rigid blocks with a thickness of 7 Å were located parallel to the GB in the Y direction. The application of an incremental shear strain induced the motion of the disconnections created at the GB, as detailed below. The disconnections cross the periodic boundary conditions (PBC) producing the annihilation of disconnections of opposite sign. This procedure impedes the pileup of disconnections at the fixed boundaries, therefore facilitating the continuous production of disconnections, as detailed in the next section, and related displacement of the GB. As a previous check, fixed BC were performed and the same mechanism of generation of disconnections was found. The difference with PBC is that the GB is bent because only the part with the source of disconnections is freely moving and pileup of disconnections is formed at the fixed boundaries.

An embedded atom method (EAM) interatomic potential for bcc-Fe developed by Mendelev *et al.* [32] has been used. The potential has been fitted to *ab initio* data and has proven to be able to describe a large number of properties involving defects in bulk bcc-Fe, namely, from small self-interstitial atom (SIA) clusters [33] to dislocations [34,35], when compared to density functional theory (DFT) results and also to experiments. The accuracy of the potential in the study of tilt ⟨110⟩ GBs was checked in [36].

IV. RESULTS AND DISCUSSION

In the following we describe the mechanism of GB displacement due to the presence of a GBD that acts as a source of disconnections. Figure 2 shows a bicrystal with the orientation of the upper (μ) crystal indicated by the blue unit

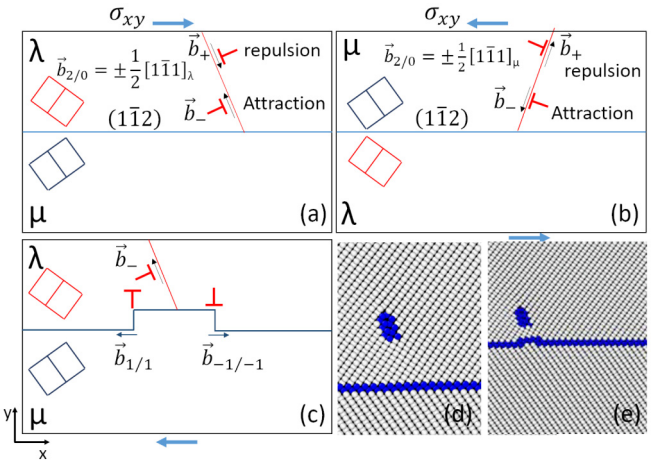

FIG. 3. (a), (b) Bicrystals showing the glide planes of crystal dislocations. The unit cell of each crystal is represented in red and blue, respectively. In this work, crystal dislocations are located in the upper crystal. (c) Interaction of the (112) GB with a crystal dislocation gliding in the λ crystal: when dislocation is close to the GB, a disconnection dipole is created. (d) Detail of the pristine GB with the crystal dislocation approaching it. (e) Detail of the simulation showing the creation of the disconnection dipole.

cell, where the axes a_1 and a_2 point inside the paper. The external shear stress parallel to the GB necessary to create a dipole $\{\vec{b}_{1/1}; \vec{b}_{-1/-1}\}$ in the pristine {112} GB is about 2.8 GPa. The strain accommodation following the creation and glide of a disconnection dipole produces a drop about 0.2 GPa while the GB moves one plane upward for $\sigma_{xy} < 0$ and downward for $\sigma_{xy} > 0$, as shown in Fig. 2. The external stress necessary to produce the shear-coupled GB migration is reduced if the creation of disconnections is facilitated by dislocation reactions at the GB.

A. Interaction of a pristine {112} GB with a $\frac{1}{2}\langle 111\rangle$ crystal dislocation

The GB-dislocation interaction depends on the orientation and sense of the Burgers vector of the dislocation. The attraction/repulsion forces acting on the crystal dislocation are image forces ($F = \frac{\Delta E}{d}$) due to the increment of enegy (ΔE) of the system when the dislocation is at a distance d of the GB [37]. The origin of ΔE is the interaction of the stress field of the dislocation with the stress field of the GB. Figures 3(a) and 3(b) show two edge dislocations $\vec{b}_{2/0} = \pm\frac{1}{2}[1\bar{1}1]$, denoted as $\vec{b}_-$ and $\vec{b}_+$, located in the μ and λ crystals, respectively, with dislocation lines along the tilt axis [110]. While $\vec{b}_-$ is attracted and absorbed by the GB, the dislocation $\vec{b}_+$ is repelled by the GB. The shear stresses at Fig. 3 push the dislocation $\vec{b}_-$ toward the GB. Reversing the stress would approach the dislocation $\vec{b}_+$ to the GB against the repulsion exerted by the GB.

1. Interaction with edge dislocation $\vec{b}_-$

Let us first consider the edge dislocation $\vec{b}_-$ that approaches the GB under an applied shear stress [Fig. 3(c)]. Initially, the system contains a flat GB and a bulk dislocation

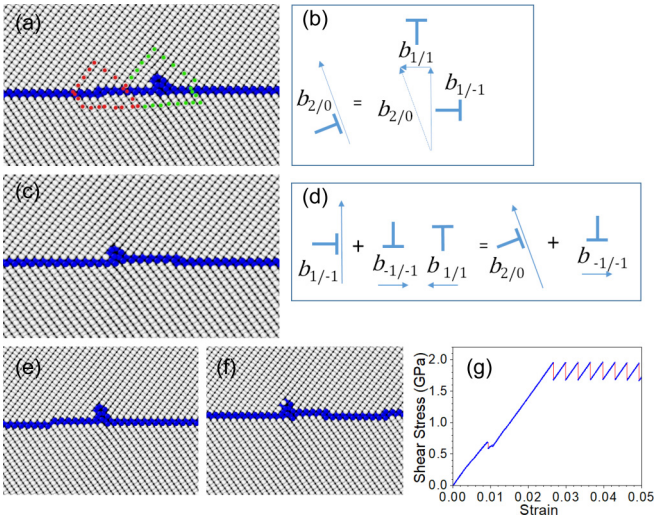

FIG. 4. (a) First decomposition of crystal dislocation into a disconnection (left) and a GB dislocation (right). Burgers circuits are indicated in red and green, respectively. (b) Analysis of the reaction shown in (a). (c), (e), (f) Emission of further disconnections: see steps at the GB. (d) Analysis of the reaction shown in (c). (g) Stress-strain curve of the process.

approaching it. When $\vec{b}_-$ is about 1 nm from the GB, a disconnection dipole is created, as shown in Figs. 3(c) and 3(e), that glides away and moves up the GB by one plane. Simultaneously, the dislocation is absorbed by the GB producing a drop of the shear stress $\Delta\sigma_{xy} = 0.15$ GPa. When the external shear stress reaches the value of $\sigma_{xy} = 2.0$ GPa, the reactions described below occur.

Step 1. $\vec{b}_{2/0}$ decomposes into a GBD that do not step the GB, $\vec{b}_{1/-1} = \frac{1}{3}[1\bar{1}2]_\lambda$, and a $\vec{b}_{1/1}$ disconnection according to the reaction $\vec{b}_{2/0} = \vec{b}_{1/1} + \vec{b}_{1/-1}$ [Fig. 4(b)]. The Burger circuits shown in Fig. 4(a) allowed identifying in the dichromatic pattern the disconnection $\vec{b}_{1/1}$ (red circuit) and $\vec{b}_{1/-1}$ (green circuit). A closed dashed line on the left of Fig. 1 shows this reaction. The GBD $\vec{b}_{1/-1}$ has a Bv perpendicular to the GB and cannot move along the GB while the disconnection $\vec{b}_{1/1}$ glides to the left under the applied shear strain. As shown in Figs. 1 and 4(b), their Bvs are at 90° and the decomposition is energetically compatible with Frank rule: $b^2_{2/0} = b^2_{1/1} + b^2_{1/-1}$, in terms of the magnitudes of Bv in units of lattice parameters: $(\frac{\sqrt{3}}{2})^2 = (\frac{\sqrt{6}}{3})^2 + (\frac{\sqrt{3}}{6})^2$. Actually, this reaction is reversible, as shown below.

Step 2. The sessile GBD $\vec{b}_{1/-1}$ acts as a stress concentrator that favors the creation of dipoles $\{\vec{b}_{1/1};\vec{b}_{-1/-1}\}$ that follow the reaction shown in Fig. 4(d): $(\vec{b}_{-1/-1} + \vec{b}_{1/1}) + \vec{b}_{1/-1} = \vec{b}_{2/0} + \vec{b}_{-1/-1}$, where $\vec{b}_{2/0}$ is created one plane above and the $\vec{b}_{-1/-1}$ runs away toward the right. Due to the length of the x direction, we can see the creation of the dipole before the first disconnection annihilates with one of the disconnections of the dipole, as shown in Fig. 4(f). All together, the GB and the crystal dislocation $\vec{b}_{2/0}$ have moved one plane up and the vicinity of $\vec{b}_{2/0}$ is identical as in step 1. In the simulation, due to the periodic boundary conditions, the disconnection dipoles coalesce. Figure 4(e) shows the emission of a $\vec{b}_{1/1}$ (step 1) and Fig. 4(f) shows the emission of $\vec{b}_{-1/-1}$ (step 2), which is about to annihilate with the image of $\vec{b}_{1/1}$ that has reentered into the system from the right. The stress-strain curve shown in Fig. 4(g) indicates that the creation of disconnection dipoles, and hence the coupled shear-GB motion, is sustained once the threshold stress is reached. A drop of stress of about 0.25 GPa is produced each time a disconnection dipole is created and glides away. The first drop of stress shown in Fig. 4(g) at a strain 0.01 corresponds to the absorption of the crystal dislocation by the GB.

The mechanism was studied by applying strain increments of 5.618×10^{-6} followed by relaxation of the system. A continuous production of disconnection dipoles at the dislocation core allowed the GB to move in the Y direction and the dislocation itself moved together with the GB along its own glide plane.

2. *Interaction with edge dislocation* $\vec{b}_+$

If the sense of the shear is reversed, the dislocation that moves toward the GB is $\vec{b}_+$ and the created dipoles swap positions (see Fig. 2), then the displacement of the GB is reversed. When $\vec{b}_+$ is at a distance of 4 nm from the GB, the repulsion between $\vec{b}_+$ and the GB provokes a local concentration of stress in the region between the dislocation and the GB of 2.48 and 2.30 GPa before and after the dipole is created, respectively. Thus, the dislocation is not absorbed, even if it does not reach the GB, but it facilitates the conservative displacement of the GB downward. In this case, the necessary external stress to trigger the GB motion is $\sigma_{xy} = 1.66$ GPa.

Therefore, a crystal edge dislocation acts as a source of disconnections that keeps the conservative motion of the GB. When the {112} GB is a coherent twin boundary, this mechanism produces either the growth or shrinkage of the twin.

3. *Interaction with mixed dislocation*

The second crystal dislocation studied has mixed character. It is denoted $\vec{b}_{1/0}$ in Fig. 1(a). Its Burgers vector $\frac{1}{2}$[1-11] can be described as the sum of $\frac{\sqrt{2}}{2}a_0$ (screw: along the tilt axis) + $0.5a_0$ (edge). The edge part, in turn, is formed by a component perpendicular to the GB and a component parallel to the GB that has a magnitude $|\vec{b}_{1/1}|$. Since the screw component is common to both crystals, a hypothetical transmission of the dislocation through the GB would need a transformation of the edge part as shown in the diagram of Fig. 1(a) (green dashed circle). This implies adding $2\vec{b}_{1/1}$ (green) disconnections. This reaction is not energetically favorable and, in fact, there is no transmission of the mixed dislocation through the GB. We checked it by performing several simulations of the interaction at $T = 0$ and 600 K, in a pristine GB and in a GB with a source of disconnections. The DP in Fig. 1(b) presents another possible reaction at the GB of the mixed dislocation. This is the decomposition into a disconnection $\vec{b}_{-1/-2}$ stepping down the GB and a disconnection $\vec{b}^{\beta}_{2/2}$. This reaction does not occur either; this is because both disconnections are sessile and they cannot go apart. The GB attracts the mixed dislocation (of

either sense) that is attached to the GB without changing its Bv. When a disconnection sweeps the GB and encounters the mixed dislocation, the lateral motion due to the pass of the disconnection corresponds to the continuous motion of the mixed dislocation in its glide plane [38]. As a result, the mixed dislocation moves along its own glide plane together with the GB in a conservative manner. In other words, the GB drags the dislocation.

There is a third crystal dislocation with Burgers vector oriented along the X axis that can be understood as a GBD with modulus exactly $3|\vec{b}_{1/1}|$ that could glide along the GB. In fact, such a dislocation does not exist at the GB because it decomposes into three disconnections and a line defect of pure step character of three planes high. The decomposition is consistent with Frank rule and it follows the conservation of Bv and step high.

These results show that only one dislocation is needed to trigger twin growth, in opposition to other proposed mechanisms such as the double cross slip growth mechanism [39] and the coalesce theory [40] that need a continuous supply of crystal dislocations to keep the GB displacement or the growth process of the {112} twin. The interaction occurs in the pristine interface, no other previous steps or disconnections are needed for the reaction to occur, as shown in Fig. 4. The fact that all the processes are conservative, no shuffles are needed and it is triggered by a single dislocation, would explain the accommodation of plastic deformation by {112} twinning at high strain rates and low temperatures. This result proves that the most complex reaction presented in [18] is not necessary and would reduce the probability of the reaction. Moreover, the complementary zonal dislocation described as $\frac{1}{3}\langle 111\rangle$ in [18] is, in fact, a disconnection $\vec{b}_{2/2}$, therefore a perfect GBD.

B. Grain boundaries vicinal to the {112} tilt GB: Behavior under shear stress

The GBs vicinal to {112} GB relax into segments of {112} GB separated by the GBD described above, $\vec{b}_{1/-1}$. The distance between GBDs depends on the $\Delta\theta$ added to the misorientation angle $\theta = 70.53^\circ$ of the {112} tilt GB, therefore, there is a maximum $\Delta\theta$ corresponding to the minimum distance between GBDs that keeps the properties of the set of vicinal GBs. Table I presents the list of vicinal GBs studied. They are indicated by the Miller indexes of the theoretical plane before relaxation; the increase of misorientation with respect to the (112) GB; the linear density of GBDs, i.e., number of GBD per unit length along the X direction; the GB energy (see Fig. 5).

TABLE I. Parameters of the vicinal GBs to the {112} GB. GBs indicated by the Miller indices of the theoretical plane before relaxation. $\Delta\theta$ is the increase of misorientation with respect to the (112) GB; the linear density of GBDs is the number of GBD per unit length along the X direction; the GB energy is plotted in Fig. 5.

GB plane	$\Delta\theta$ (degrees)	Linear density of GBD (nm^{-1})	GB energy (J/m^2)
(112)	0	0	0.245
Σ1681 (23, 23, 48)	−2.28	0.154	0.418
Σ1161 (19, 19, 40)	−2.74	0.205	0.433
Σ417 (8, 8, 17)	−3.22	0.242	0.451
Σ113 (4, 4, 9)	−6.22	0.466	0.499
Σ97 (5, 5, 12)	−9.51	0.711	0.570
Σ33 (2, 2, 5)	−11.53	0.862	0.595

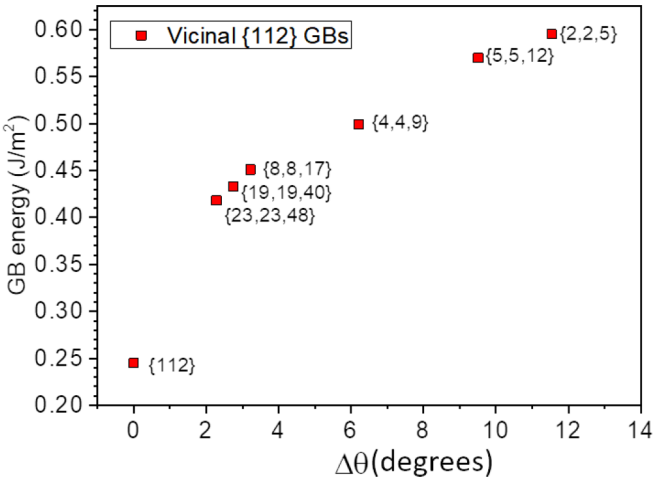

FIG. 5. GB energy of the GBs vicinal to {112} as a function of increase of misorientation. The planes indicated with Miller indices correspond to the GBs before relaxation into segments of {112} separated by GBDs.

In Fig. 6(a) we present the vicinal GB (19, 19, 40) corresponding to $\Delta\theta = -2.74^\circ$. The distance between GBDs is $D = \frac{b_{1/-1}}{2\sin\frac{\Delta\theta}{2}} = 20\frac{\sqrt{3}}{2}a_0$. Figure 6(b) is a pressure map of the GB showing the regions of tension (blue) and compression (red) of the GBDs.

When the GB is under an applied shear stress, each of the GBDs acts as a source of dipoles of $\vec{b}_{1/1}$ disconnections

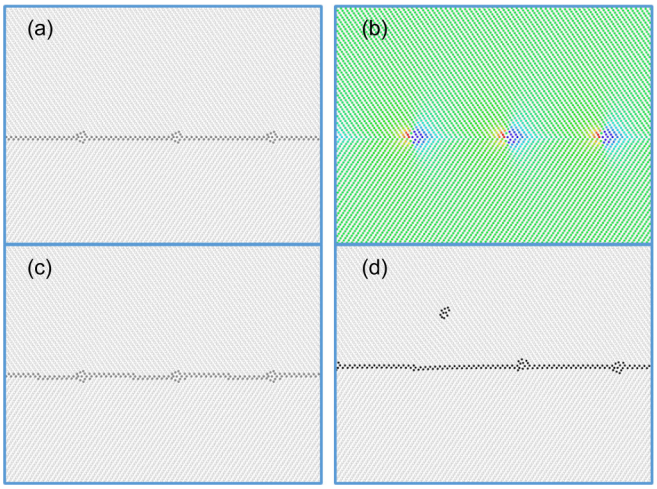

FIG. 6. (19, 19, 40) GB vicinal to {112}. (a) GB in equilibrium formed by GBDs and segments of {112} GB. (b) Pressure map. (c) GB under shear stress: disconnections are running toward the right from one GBD to the next. (d) GB under a high strain rate: emission of a dislocation (see text for details).

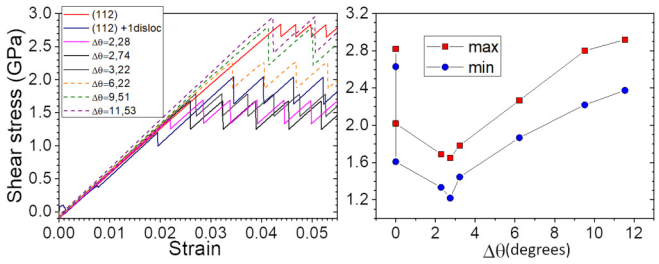

FIG. 7. Shear stress applied to the {112}GB, {112}GB + 1 dislocation, and its vicinal GBs. (a) Strain-stress curves. (b) Shear stress necessary for the displacement of the GB (max) and shear stress after the emission of disconnections (min) versus the increment of misorientation defining the vicinal GBs.

and the reaction shown in Fig. 4(d) occurs at each GBD [see Fig. 6(c)] that transforms into $\vec{b}_{2/0} + \vec{b}_{-1/-1}$. The disconnection $\vec{b}_{-1/-1}$ runs toward the next $\vec{b}_{2/0}$ dislocation, that transforms back to $\vec{b}_{1/-1}$. As a result, the GB has moved two planes up and each GBD has moved with the GB. All together is a conservative motion that occurs at a stress $\sigma_{xy} = -1.67$ GPa. The process reaches a steady state with drops of about 0.4 GPa for each displacement of the GB.

To check the efficiency of the mechanism under high strain rates we applied $\dot{\varepsilon} = 10^{10}$ s^{-1}. We observed that some crystal dislocations may jump out the GB up to few lattice parameters [see Fig. 6(d)]. At $T = 0$ K the process is unstable and they return to the GB (stable position), as it would happen with the dislocations that form a low-angle GB since the GB is the position of lowest energy for these GBDs.

The properties of the vicinal GB described above are kept up to a distance between $b_{1/-1}$ of about $5\frac{\sqrt{3}}{2}a_0$ that corresponds to $\Delta\theta = -11.536^\circ$. In Fig. 7(a) we present the stress-strain curves for the vicinal GBs studied; the curve for the pristine (112) GB and the (112) GB after absorption of a crystal dislocation are included for comparison. We observe that the stress necessary to move the vicinal GBs under a shear-coupled migration up to $\Delta\theta = -6.22^\circ$ is lower than the stress for the pristine GB. This is due to the presence of GBDs that act as sources of disconnections. For higher $\Delta\theta$ the number of GBDs demands a stress comparable to the pristine GB but the mechanism of creation of disconnection dipoles still applies. Figure 7(b) shows the maximum stress necessary to create the dipole of disconnections (red dots) that keeps the displacement of the GB in a steady state and the minimum stress (blue dots) reached after the drop due to the motion of disconnections. The curve has a minimum value of 1.67 GPa for the (19,19,40) GB, for which the efficiency of disconnection sources is maximum.

Thus, GBs vicinal to {112} GB can perform a shear-coupled GB migration more efficiently with lower stress in a fully conservative process. In Fig. 8 we present three examples of vicinal GBs. Figures 8(a) and 8(b) present GBs with low and high GBD density, respectively. Figures 8(c) and 8(d) capture two frames of the motion of a (5,5,12) GB under a strain rate of $\dot{\varepsilon} = 10^{10}$ s^{-1}. There are two and four steps, respectively, corresponding to the disconnections running toward the right. In this case, the distribution of stresses is not uniform and not all sources are activated at the same time.

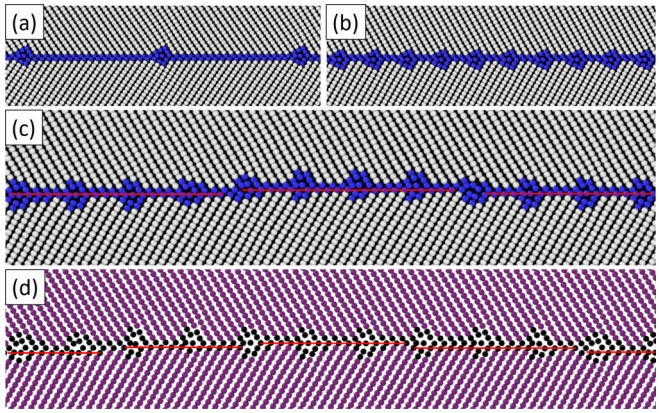

FIG. 8. (a) (19,19,40) GB, (b) (2,2,5) GB, (c), (d) snapshots of (5,5,12) under high strain rate: inhomogeneous creation of disconnections.

Even in this extreme case, the process is fully conservative and the process at each GBD is as described above. This implies that the role of the $\vec{b}_{1/-1}$ GBD is important in the accommodation of plastic deformation of polycrystalline metals with bcc structure because it concerns the conservative growth of twins, the conservative displacement of {112} GBs, and all its vicinal GBs.

V. SUMMARY AND CONCLUSIONS

We describe a mechanism of plastic deformation in bcc metals associated to the shear-coupled grain-boundary migration of the {112} tilt GB and the GBs vicinal to the {112} GB. The mechanism is directly applicable to the {112} twin boundary and governs the growth and shrinkage of the twin.

The shear-coupled GB migration is produced by the creation and glide of disconnections. These disconnections may be created directly at the pristine GB or may be created, at lower stress, by a source of disconnections, which is the GBD $\vec{b}_{1/-1}$ described in this work. This GBD is created at the GB by the interaction of the GB with an edge dislocation with Burgers vector $\vec{b} = \frac{1}{2}\langle 111\rangle$. Moreover, this GBD appears at the GBs vicinal to the {112} GB due to the relaxation of the GB into segments of {112} orientation separated by $\vec{b}_{1/-1}$ GBDs. Under stress, these GBD act as sources of disconnections and the vicinal GB is displaced by the same mechanism. The fact that the crystal dislocation decomposes, in a reversible way, into $\vec{b}_{1/-1}$ plus the disconnection responsible for the motion of the GB is essential to have a conservative process. Thus, the mechanism described accommodates efficiently plastic deformation since no residual defects are left behind in the displacement of the GBs and no atomic diffusion is needed during the whole process.

Finally, the interaction of the symmetric $\{112\}\langle 110\rangle$ tilt GB with the family of $\frac{1}{2}\langle 111\rangle$ crystal dislocations depends on the orientation of the dislocation. While the edge dislocation produces a source of disconnections, the mixed dislocation keeps its own Burgers vector and it is dragged by the GB during its shear-coupled GB migration. Both dislocations are absorbed by the GB and no transmission to the next grain is produced.

To conclude, the (112)GB and vicinal GBs accommodate plastic deformation by shear-coupled GB migration. The same mechanism is applied to the growth and shrink of (112) twins.

ACKNOWLEDGMENTS

This work was supported by the Euratom research and training programme 2014–2018 under Grant Agreement No. 755039 (Project M4F), by the Spanish MINECO: Grants No. FIS2015-69017-P and No. RTI2018-096006-B-I00, the latter with ERDF funds. This work also contributes to the Joint Program on Nuclear Materials (JPNM) of the European Energy Research Alliance (EERA). Simulations partially carried out in the computing facilities provided by the CYTED Network RICAP (517RT0529).

[1] A. J. Haslam, D. Moldovan, V. Yamakov, D. Wolf, S. R. Phillpot, and H. Gleiter, Stress-enhanced grain growth in a nanocrystalline material by molecular-dynamics simulation, Acta Mater. **51**, 2097 (2003).

[2] J. W. Cahn, Y. Mishin, and A. Suzuki, Coupling grain boundary motion to shear deformation, Acta Mater. **54**, 4953 (2006).

[3] D. S. Gianola, S. Van Petegem, M. Legros, S. Brandstetter, H. Van Swygenhoven, and K. J. Hemker, Stress-assisted discontinuous grain growth and its effect on the deformation behavior of nanocrystalline aluminum thin films, Acta Mater. **54**, 2253 (2006).

[4] F. Mompiou, D. Caillard, and M. Legros, Grain boundary shear-migration coupling. I. In situ TEM straining experiments in Al polycrystals, Acta Mater. **57**, 2198 (2009)

[5] T. Gorkaya, D. A. Molodov, and G. Gottstein, Stress-driven migration of symmetrical ⟨100⟩ tilt grain boundaries in Al bicrystals, Acta Mater. **57**, 5396 (2009).

[6] D. A. Molodov, T. Gorkaya, and G. Gottstein, Dynamics of grain boundaries under applied mechanical stress, J. Mater. Sci. **46**, 4318 (2011).

[7] A. Rajabzadeh, M. Legros, N. Combe, F. Mompiou, and D. A. Molodov, Evidence of grain boundary dislocation step motion associated to shear-coupled grain boundary migration, Philos. Mag. **93**, 1299 (2013).

[8] A. Rajabzadeh, F. Mompiou, S. Lartigue-Korinek, N. Combe, M. Legros, and D. A. Molodov, The role of disconnections in deformation-coupled grain boundary migration, Acta Mater. **77**, 223 (2014)

[9] N. Combe, F. Mompiou, and M. Legros, Disconnections kinks and competing modes in shear-coupled grain boundary migration, Phys. Rev. B **93**, 024109 (2016)

[10] H. A. Khater, A. Serra, R. C. Pond, and J. P. Hirth, The disconnection mechanism of coupled migration and shear at grain boundaries, Acta Mater. **60**, 2007 (2012).

[11] A. Rajabzadeh, F. Mompiou, M. Legros, and N. Combe, Elementary Mechanisms of Shear-Coupled Grain Boundary Migration, Phys. Rev. Lett. **110**, 265507 (2013).

[12] K. D. Molodov, T. Al-Samman, D. A. Molodov, and S. Korte-Kerzel, On the twinning shear of (1012) twins in magnesium: Experimental determination and formal description, Acta Mater. **134**, 267 (2017).

[13] A. Serra and D. J. Bacon, A new model for {10-12} twin growth in hcp metals, Philos. Mag. A **73**, 333 (1996).

[14] N. Combe, F. Mompiou, and M. Legros, Heterogeneous disconnection nucleation mechanisms during grain boundary migration, Phys. Rev. Mater. **3**, 060601 (2019)

[15] P. D. Bristowe and A. G. Crocker, A computer simulation study of the structure of twinning dislocations in body centered cubic metals, Acta Metall. **25**, 1363 (1977).

[16] Y. Cheng, M. Mrovec, and P. Gumbsch, Atomistic simulations of interactions between the 1/2 ⟨111⟩ edge dislocation and symmetric tilt grain boundaries in tungsten, Philos. Mag. **88**, 547 (2008).

[17] M. Mrovec, C. Elsässer, and P. Gumbsch, Interactions between lattice dislocations and twin boundaries in tungsten: A comparative atomistic simulation study, Philos. Mag. **89**, 3179 (2009).

[18] B. Jiang, A. Tu, H. Wang, H. Duan, S. He, H. Ye, and K. Du, Direct observation of deformation twinning under stress gradient in body-centered cubic metals, Acta Mater. **155**, 56 (2018).

[19] R. C. Pond, *Dislocations in Solids*, Vol. 8 (Elsevier, Oxford, 1989).

[20] J. P. Hirth, Dislocations, steps and disconnections at interfaces, J. Phys. Chem. Solids **55**, 985 (1994).

[21] J. P. Hirth and R. C. Pond, Steps, dislocations and disconnections as interface defects relating to structure and phase transformations, Acta Mater. **44**, 4749 (1996).

[22] A. Sutton and R. Balluffi, *Interfaces in Crystalline Materials* (Clarendon, Oxford, 1996).

[23] G. S. Was, *Fundamentals of Radiation Materials Science* (Springer, New York, 2007).

[24] M. A. Tschopp, K. N. Solanki, F. Gao, X. Sun, M. A. Khaleel, and M. F. Horstemeyer, Probing grain boundary sink strength at the nanoscale: Energetics and length scales of vacancy and interstitial absorption by grain boundaries in α-Fe, Phys. Rev. B **85**, 064108 (2012).

[25] M. Rajagopalan, M. A. Tschopp, and K. N. Solanki, Grain boundary segregation of interstitial and substitutional impurity atoms in alpha-iron, JOM **66**, 129 (2014).

[26] J. W. Christian and S. Mahajan, Deformation twinning, Prog. Mater. Sci. **39**, 1 (1995).

[27] J. P. Hirth, R. C. Pond, and J. Lothe, Spacing defects and disconnections in grain boundaries, Acta Mater. **55**, 5428 (2007).

[28] H. A. Khater, A. Serra, and R. C. Pond, Atomic shearing and shuffling accompanying the motion of twinning disconnections in Zirconium, Philos. Mag. **93**, 1279 (2013).

[29] N. Anento and A. Serra, Interaction of a mobile {112} grain boundary with radiation induced defects in α-Fe: transformation of defects and impact on the shear-coupled grain boundary migration, Comput. Mater. Sci. **179**, 109679 (2020).

[30] S. Plimpton, Fast parallel algorithms for short-range molecular dynamics, J. Comput. Phys. **117**, 1 (1995).

[31] A. Stukowski, Efficient implementation of the concentration-dependent embedded atom method for molecular-dynamics and Monte-Carlo simulations, Modell. Simul. Mater. Sci. Eng. **18**, 015012 (2009).

[32] G. Ackland, M. I. Mendelev, D. J. Srolovitz, S. Han, and A. V. Barashev, Development of an interatomic potential for phosphorus impurities in α-iron, J. Phys.: Condens. Matter **16**, S2629 (2004).

[33] F. Willaime, C. C. Fu, M. C. Marinica, and J. Dalla Torre, Stability and mobility of self-interstitials and small interstitial clusters in α-iron: Ab initio and empirical potential calculations, Nucl. Instrum. Methods Phys. Res., B **228**, 92 (2005).

[34] C. Domain, G. Monnet, Simulation of Screw Dislocation Motion in Iron by Molecular Dynamics Simulations, Phys. Rev. Lett. **95**, 215506 (2005).

[35] H. A. Khater, G. Monnet, D. Terentyev, and A. Serra, Dislocation glide in Fe-carbon solid solution: From atomistic to continuum level description, Int. J. Plast. **62**, 34 (2014).

[36] D. Terentyev, X. He, A. Serra, and J. Kuriplach, Structure and strength of $\langle 110 \rangle$ tilt grain boundaries in bcc Fe: An stomistic study, Comput. Mater. Sci. **49**, 419 (2010).

[37] O. Kallfallah, M. Condat, and L. Priester, Image force on a lattice dislocation due to a grain boundary in bcc metals, Philos. Mag. A **67**, 231 (1993).

[38] R. C. Pond, A. Serra, and D. J. Bacon, Dislocations in interfaces in hcp metals: II Mechanisms of defect mobility under stress, Acta Mater. **47**, 1441 (1999).

[39] C. Q. Chen, G. Hu, J. N. Florando, M. Kumar, K. J. Hemker, and K. T. Ramesh, Interplay of dislocation slip and deformation twinning in tantalum at high strain rates, Scr. Mater. **69**, 709 (2013).

[40] S. Mahajan, Interrelationship between slip and twinning in B. C. C. crystals, Acta Metall. **23**, 671 (1975).